Journal of Energy Chemistry 71 (2022) 612–618

Contents lists available at ScienceDirect

Journal of Energy Chemistry

journal homepage: www.elsevier.com/locate/jechem

http://www.journals.elsevier.com/journal-of-energy-chemistry/

Dry electrode technology for scalable and flexible high-energy sulfur cathodes in all-solid-state lithium-sulfur batteries

Jiang-Kui Hu [a,b], Hong Yuan [a,b,*], Shi-Jie Yang [a,b], Yang Lu [c], Shuo Sun [c], Jia Liu [d], Yu-Long Liao [a,b], Shuai Li [a,b], Chen-Zi Zhao [c,*], Jia-Qi Huang [a,b]

[a] School of Materials Science & Engineering, Beijing Institute of Technology, Beijing 100081, China
[b] Advanced Research Institute of Multidisciplinary Science, Beijing Institute of Technology, Beijing 100081, China
[c] Beijing Key Laboratory of Green Chemical Reaction Engineering and Technology, Department of Chemical Engineering, Tsinghua University, Beijing 100084, China
[d] Beijing Key Laboratory of Lignocellulosic Chemistry, Beijing Forestry University, Beijing 100083, China

ARTICLE INFO

Article history:
Received 14 April 2022
Revised 28 April 2022
Accepted 28 April 2022
Available online 7 May 2022

Keywords:
All-solid-state lithium-sulfur batteries
Sulfide solid electrolytes
Sheet-type electrodes
Composite sulfur cathode
Dry electrode technology

ABSTRACT

All-solid-state lithium-sulfur batteries (ASSLSBs) employing sulfide solid electrolytes are one of the most promising next-generation energy storage systems due to their potential for higher energy density and safety. However, scalable fabrication of sheet-type sulfur cathodes with high sulfur loading and excellent performances remains challenging. In this work, sheet-type freestanding sulfur cathodes with high sulfur loading were fabricated by dry electrode technology. The unique fibrous morphologies of polytetrafluoroethylene (PTFE) binders in dry electrodes not only provides excellent mechanical properties but also uncompromised ionic/electronic conductance. Even employed with thickened dry cathodes with high sulfur loading of 2 mg cm^{-2}, ASSLSBs still exhibit outstanding rate performance and cycle stability. Moreover, the all-solid-state lithium-sulfur monolayer pouch cells (9.2 mAh) were also demonstrated and exhibited excellent safety under a harsh test situation. This work verifies the potential of dry electrode technology in the scalable fabrication of thickened sulfur cathodes and will promote the practical applications of ASSLSBs.

1. Introduction

The pursuit for the sustainable development of society and the goal of carbon neutrality propels the unremitting innovation of energy technologies [1–6]. However, conventional electrode preparation of rechargeable batteries is mainly based on a scalable wet-slurry casting process, which is energy consumption and time-consuming. Besides, the use of toxic organic solvents also causes healthy and environmental concerns [7]. Dry electrode technology, a more promising technique to accommodate future sustainability, has drawn numerous attention recently [8–10]. Compared with the conventional wet-slurry casting process, solvent-free dry electrode technology can eliminate the use of toxic organic solvents and simplify the manufacturing process. In particular, the dry electrode technology shows attractive prospects in thick electrode preparation for high-energy–density batteries [11,12]. On one hand, a solvent-free process can circumvent the cracking and delamination of thick electrodes resulting from the volatilization of organic solvent. On the other hand, the dry electrode process can significantly decrease the amount of inert binder and regulate its distribution and thus, mitigating binder surface coating on active materials to block ion conduction and ensuring the efficient transportation of Li-ion [13–15].

All-solid-state batteries (ASSBs) adopting inorganic solid-state electrolytes to replace organic liquid electrolytes are considered as one of the next-generation revolutionary battery batteries [16–21], among which sulfide-based all-solid-state lithium-sulfur batteries (ASSLSBs) further become a rising star due to their ultra-high theoretical energy density (2600 Wh kg^{-1}) and intrinsic safety [22–28]. However, sulfide electrolyte materials with high ionic conductivity are highly reactive or easy to dissolve with/in commonly polar solvents, which results in a tremendous discrepancy between the selection of sulfide electrolytes for nonpolar or less polar solvents and the need for polymer binders for dissolution in polar solvents [29–34]. Therefore, the preparation of large-scale and sheet-type solid-state sulfur cathodes is usually restricted through a conventional wet-slurry casting process owing to the incompatibilities between dispersion solvents, sulfide

* Corresponding authors.
E-mail addresses: yuanhong@bit.edu.cn (H. Yuan), zcz@mail.tsinghua.edu.cn (C.-Z. Zhao).

https://doi.org/10.1016/j.jechem.2022.04.048

electrolytes and binders. In contrast, solvent-free dry electrode technology opens a light space for ASSLSBs [35–37].

Recently, a simple dry method process has been used to prepare an ultrathin sulfide solid electrolyte membrane and proves the effectiveness of this emerging technique in ASSBs [38]. Compared with simplified components in electrolyte membranes, free-standing sheet-type composite dry-cathode membranes, consisting of active material ($LiNi_{0.9}Co_{0.05}Mn_{0.05}O_2$, NCM), conductive carbon, Li_6PS_5Cl electrolyte and polytetrafluoroethylene (PTFE) binder were reported by Hippauf et al. [39]. The cathode membrane with only 0.3 wt% binders exhibited considerable mechanical strength. Unprecedentedly, a prominent breakthrough of practical Ah-level pouch cells with a high energy density (>900 Wh L^{-1}) and superior cycle life (>1000 times) has been achieved by Samsung mainly ascribing to the dry-method thick electrodes [40]. These results indicate the huge potential of the dry electrode technology application in high-energy–density ASSLSBs. However, different from traditional intercalation-type NCM cathodes with relatively high electronic and ionic conductivities, the rigorous requirement of solid-state sulfur cathodes for the mixed conduction of Li ions and electrons makes ASSLSBs more challengeable due to the insulative nature of sulfur and its discharge product Li_2S [41,42]. Currently, research on ASSLSBs is still staying at a lab mold scale due to the lack of large-scale sheet-type sulfur cathodes [43–47]. Therefore, it is urgent to exploit the scalable preparation of solid-state sulfur cathode and thus, promoting the development of ASSLSBs.

Herein, a sheet-type composite sulfur cathode was prepared by dry electrode technology. Benefiting from low content (1 wt%) and unique fibrous distribution of binder, the solid-state composite sulfur cathode exhibited excellent mechanical properties and rapid ionic/electronic transportation. Combining with Li_6PS_5Cl solid electrolytes and Li anodes, the all-solid-state lithium-sulfur mold cells showed outstanding rate performance and enhanced cycle stability even under the condition of high sulfur loading of 2 mg cm^{-2}. In terms of the capability of the dry-electrode process in the large-scale preparation of sulfur cathode, the all-solid-state lithium-sulfur pouch cells are also demonstrated.

2. Experimental

2.1. Preparation of sheet-type composite sulfur cathodes

The freestanding sheet-type composite sulfur cathodes were prepared based on dry electrode technology. The composite sulfur cathode powders (S:C:Li_6PS_5Cl = 1:1:2 by weight) were firstly prepared referring to the previous work [45]. Then, the obtained composite sulfur cathode powders were mixed with PTFE (Daikin Fluorochemicals (China) Co., Ltd) binder. After 5 min of grinding, the mixture was placed on a stainless steel plate and rolled out. The wet-slurry casting composite sulfur electrodes used silicone rubber (SR) as binders and n-hexane as solvents. All the above processes were carried out in a dry Ar-filled glove box (O_2 < 0.1 ppm, H_2O < 0.1 ppm).

2.2. Material characterization

The morphologies of samples were characterized by the field-emission scanning electron microscope (JEOL, JSM 7401F). The sulfur content was determined by thermo-gravimetric analysis (NETZSCH, STA-449F3) under dry N_2 flow with a heating rate of 10 °C min^{-1}. X-ray diffraction (XRD) measurements of samples were carried out using a Bruker D8 diffractometer with a Cu-Kα radiation in a 2θ range of 10°–60° at 5° min^{-1}. Kapton tape was used to cover the samples to isolate the oxygen and water in the atmosphere. The mechanical properties of the sheet-type composite sulfur cathodes were investigated by a Zwick testing machine at a stretching speed of 1 mm min^{-1} at room temperature. The chemical compositions before and after cycling of the sheet-type composite sulfur cathodes were analyzed using X-ray photoelectron spectroscopy (Kratos Analytical, Axis Supra+) with an Al *K*α line as the X-ray source. The samples were directly transferred from a glovebox to the analysis chamber to avoid contact with air.

2.3. Cell assembly

The all-solid-state mold cells were fabricated as the following procedures: Firstly, the Li_6PS_5Cl (100 mg) was cold-pressed in a poly(ether-ether-ketone) (PEEK) mold under 360 MPa. Then, the composite sulfur cathode was pressed on one side of the electrolyte under 360 MPa. Finally, the Li foil (100 μm) as the anode was attached to the other side. As for the pouch cells, the composite sulfur cathode (2 × 3 cm^2) and solid electrolyte sheet (2.5 × 3.5 cm^2) were firstly stacked and pressurized by the cold isostatic press. Then a lithium foil (2.2 × 3.2 cm^2) was pasted on the opposite side of the solid electrolyte sheet. In addition, the lugs are prewelded on the current collector through an ultrasonic welding machine. It is worth noting that the solid electrolyte sheet was prepared by the same dry electrode technology and it is a mixture of Li_6PS_5Cl solid electrolyte and PTFE (99:1 by weight).

2.4. Electrochemical performance measurements

The Li-ion conductivities of the composite sulfur cathodes with different PTFE contents were measured using an alternating current (AC) impedance method by a Solartron Energy Lab XM. The EIS measurements were conducted using a Li/SE/cathodes/SE/Li cell configuration in a frequency range from 1 MHz to 0.1 Hz with an amplitude of 10 mV [48]. A sandwich cell of stainless steel (SS)/-cathodes/stainless steel (SS) was used to test the electronic conductivity of the samples on a Solartron 1470E electrochemical workstation by direct current (DC) polarization method with a constant voltage of 100 mV. The cyclic voltammetry (CV) was conducted with a scanning rate of 0.1 mV s^{-1} between 1 ∼ 3 V (vs. Li/Li^+) on the same workstation. Galvanostatic charge–discharge tests were carried out on the LAND testing system (Wuhan LAND Electronics Co., Ltd.) in the voltage range of 1.5 ∼ 2.8 V (vs.Li/Li^+).

3. Results and discussion

The ionic/electronic transport completely relies on solid–solid contact in all-solid-state batteries, while different electrode preparation processes will lead to different binder distributions and electrode microstructures. In conventional wet-slurry-produced electrodes, the binder is generally coated on the surface of the active material, which will block the direct contact between electrode particles and eventually limit the interfacial transport of Li ions and electrons. Moreover, high binder content must be used to obtain satisfactory mechanical performance. While in emerging solvent-free produced dry electrodes, the binders exhibit a three-dimensional fibrous network connection under the function of shear force, which can remain the directly intimate contact between active materials and solid electrolytes/conductive agents and thus ensure rapid ionic/electronic transportation and high mechanical performances, as shown in Fig. 1(a). Fig. 1(b) shows the morphology of sheet-type composite sulfur cathodes via the dry electrode process. The electrode particles are connected to each other through fibrous PTFE binders. Besides, the corresponding EDS mapping images show evenly distributed S, C, P and F elements in sulfur cathodes, which confirms the uniform distribution

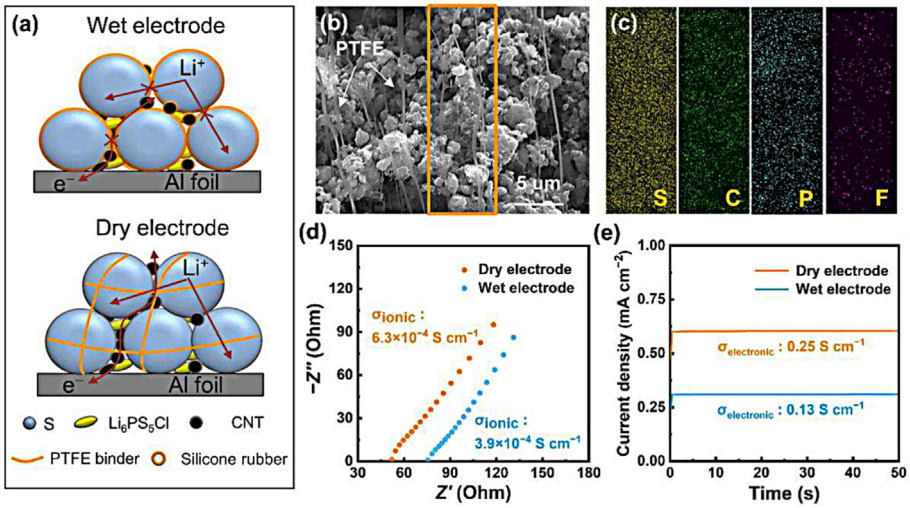

Fig. 1. (a) Schematic diagrams of electrode microstructures by conventional wet-slurry casting and dry electrode technology. SEM images of the sheet-type sulfur cathode (b) and (c) corresponding EDS mapping of S, C, P and F elements marked in (b). (d) EIS curves and (e) current–time plots of dry and wet composite sulfur cathodes with 1 wt% binders.

of the S/C composites, Li_6PS_5Cl and PTFE (Fig. 1c). After pressurization, the dry electrode becomes dense (Fig. S1). In contrast, the active materials in wet-slurry casted electrodes are largely covered by inert binder layers and therefore, resulting in impeded ionic/-electronic transportation (Fig. S2). The DC and AC tests of composite electrodes further demonstrated the advantages of dry electrodes in ionic and electronic conduction (Fig. 1d and e). In terms of both electrodes with the same binder content, the dry electrodes show 61.5% increased ionic conductivity and 100% elevated electronic conductivity due to the distinct fibrous PTFE distribution.

The amount of sulfur in the S/C composite was determined by thermogravimetric analysis (TGA) under N_2 atmosphere (Fig. S3). The weight loss of S/C composite is approximately 49.9%, which is in agreement with the content of sulfur. In order to confirm the compatibility between electrode materials in the solid-state sulfur cathodes, X-ray diffraction (XRD) patterns were conducted. There are no obvious diffraction peaks in S/C composites (Fig. S4), indicating the amorphous structure of sulfur in the S/C composite [49]. In addition, the crystal structure of Li_6PS_5Cl remains unchanged, which means no significant side reactions between Li_6PS_5Cl, S/C composite and PTFE during the dry-milling process (Fig. S5). It's worth noting that the diffraction peak at 2 theta of around 20° is corresponding to the sealing tape used to separate the sample from the air.

Generally, the solid-state cathode is mainly composed of inorganic rigid solid powders, which have poor elasticity and weak bonding ability. The conventional cold-pressed solid-state powder electrode plates exhibit fragile and are easy to be broken. Therefore, solid electrode films with outstanding mechanical strength are of great significance for scalable processing. Benefiting from the unique advantage in fibering properties of PTFE under shear force, solid electrodes by a dry process can easily maintain intimate interfacial contact through the three-dimensional fibrous network connection even with a low PTFE binder. As-prepared sheet-type composite sulfur cathodes (4×10 cm^2) via dry electrode technology with different contents of PTFE are presented in Fig. 2. Due to the flexible nature of PTFE binder fibers, all the cathodes exhibit good flexibility and can be folded even reducing binder content to 0.5 wt%. However, when the binder content decreases to 0.5 wt%, the sulfur electrode film will be torn when lifted by tweezers. As a comparison, the wet-slurry casting sulfur electrodes need more amount of binder (~5 wt%) to achieve similar mechanical properties (Fig. S6).

In order to further quantitate the effect of binder content on the mechanical properties of dry electrodes, tensile tests were performed. As shown in Fig. 3(a) and Fig. S7, the tensile strengths increase from 0 to 126 kPa with increasing PTFE content from 0.5 wt% to 10 wt%. All sulfur cathode films exhibit prominent transferability, which is a pivotal evaluation criterion for an electrode as well as battery processing, except the electrode film with 0.5 wt% PTFE. In addition, the ambient Li-ion conductivity and electronic conductivity of the electrode films were investigated (Fig. 3b and Table S1). It is clearly accepted that the ionic/electronic conductivities decrease with increasing inert binder content. However, due to the superiority in binder fibrous distribution in dry electrode films, the ionic and electronic conductivities for the electrode film with 1 wt% PTFE are 6.3×10^{-4} S cm^{-1} and 0.25 S cm^{-1}, respectively, while which are 7.6×10^{-4} S cm^{-1} and 0.31 S cm^{-1} for pristine powder electrode. Therefore, the introduction of appropriate binder content in dry electrodes will not offer an obvious compromise of charge transport kinetics.

Cyclic voltammogram (CV) measurements were further conducted to investigate the influence of PTFE binder content on reaction kinetics (Fig. 3c). The remarkable peaks at around 1.7 V and 2.6 V are attributed to S oxidation and Li_2S reduction, respectively. It can be seen that the redox current densities for electrodes decrease with the increase of binder contents. However, when the binder content in the dry electrode increases from 1 wt% to 10 wt%, the amount of active material only reduces by about 2 wt%. In contrast, the redox current density decreases by more than 50%, implying the sharply deteriorated sulfur reaction kinetics mainly originating from the high content of binders. These results are corresponding to the fact that high binder contents will impede the intimate contact between electrode materials and thus improve the tortuosity for ionic transport. Compared with sulfur electrodes with other contents, the electrode with 1 wt% PTFE shows stronger redox peak current densities, which are comparable with that of powder sulfur electrode, indicating better reaction kinetics. Therefore, taking comprehensive mechanical and electrochemical properties into consideration, the dry electrode with 1 wt % PTFE content is chosen as an ideal sulfur electrode for full cells.

The rate performances of ASSLSBs employing sheet-type sulfur cathodes with varied PTFE content were evaluated to further

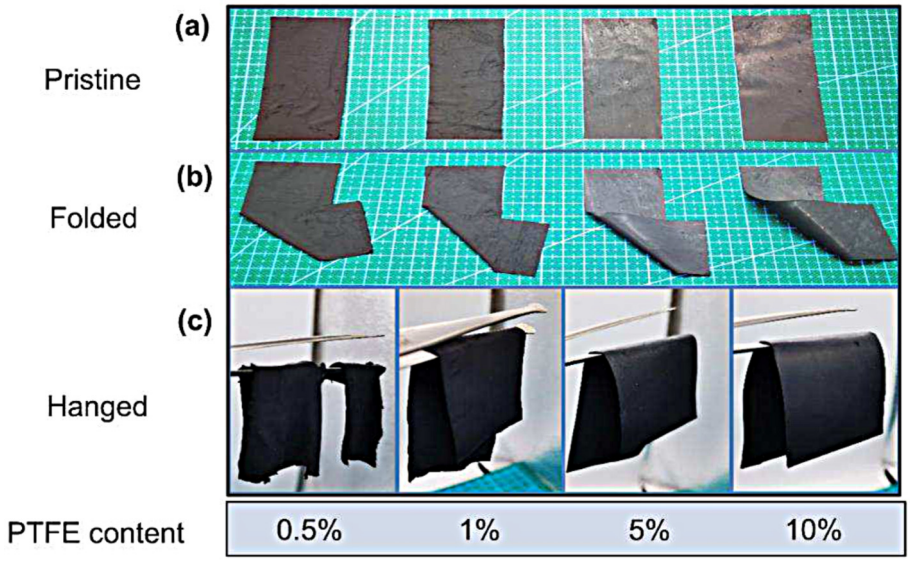

Fig. 2. Digital photographs of (a) pristine, (b) folded and (c) lifted sheet-type free-standing dry electrode membranes with different PTFE contents.

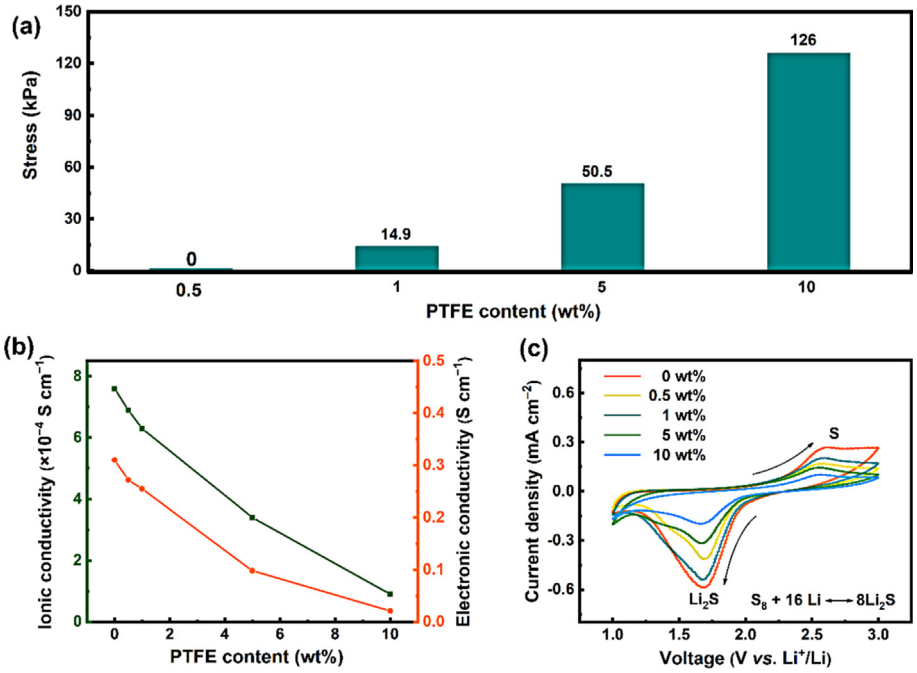

Fig. 3. (a) Stress values, (b) electronic/ionic conductivities and (c) cyclic voltammetry curves of cold-pressed powder sulfur cathode and dry-method produced cathodes with different PTFE contents.

confirm enhanced electrochemical performances (Fig. 4a). The ASSLSBs with a configuration of Li metal as anodes, Li_6PS_5Cl as electrolytes and dry electrode films as sulfur cathodes were implemented in mold cells under a stack press of 10 MPa. Toward dry-produced sulfur electrode sheets with 1 wt% PTFE (S/C/LPSC sheet-type cathode), high reversible discharge capacities of 932.2, 890.8 and 780 mAh g^{-1} are obtained at the rate in the order of 0.05 C, 0.1 C and 0.2 C, respectively. Continually increasing the current density to a high rate of 0.3 C, a high discharging capacity of 665.1 mAh g^{-1} is achieved, which is even higher than that (616.1 mAh g^{-1}) of powder cathode without PTFE binder (S/C/LPSC powder cathode). Besides, when reversing the current density back to 0.05C, a high-capacity recovery of 873.9 mAh g^{-1} is obtained, which is 93.7% of the initial discharge capacity. In contrast, despite higher initial discharge capacities, only 88.2% of the initial discharge capacity is reverted for powder cathode. Enhanced rate performances indicate improved electrochemical kinetics. On one hand, low PTFE binder content in sheet-type dry cathodes has a negligible influence on ionic and electronic transport. On the other hand, the fibrous structure of PTFE binders ensures close contact between active materials and mitigates the stress and strain resulting from the change in volume during sulfur electrochemical conversion. The corresponding charge–discharge voltage profiles further prove the feasibility of dry electrode technology. The sheet-type cathodes deliver a lower charging polarization at 0.3 C, indicating

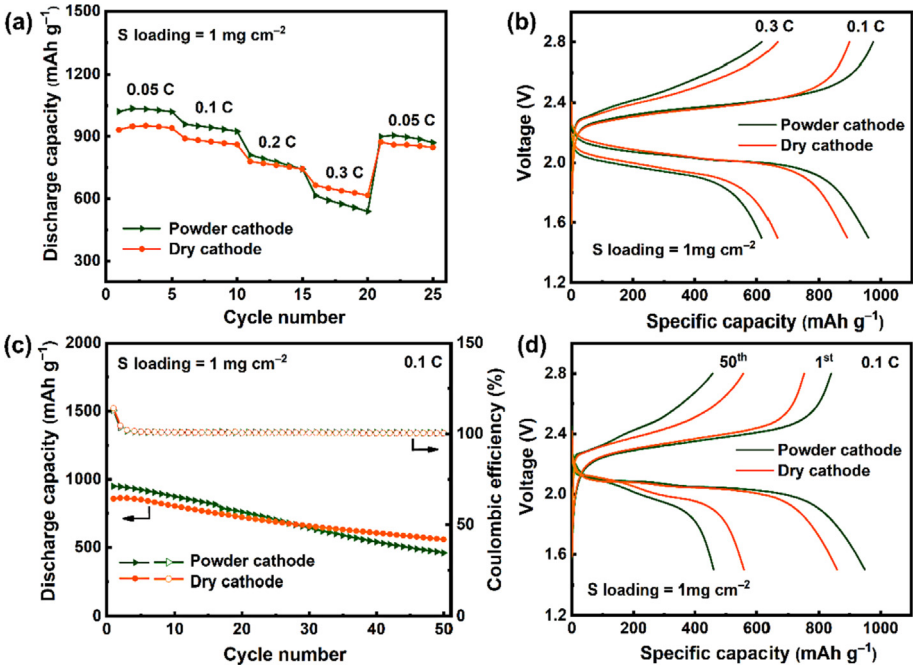

Fig. 4. (a) Rate performance and (b) corresponding charge–discharge voltage profiles, and (c) cycling performances and (d) corresponding charge–discharge voltage profiles of ASSLSBs with powder cathodes and sheet-type dry electrodes. All batteries were measured at 0.1 C and 60 °C. The sulfur loading is 1 mg cm^{-2}.

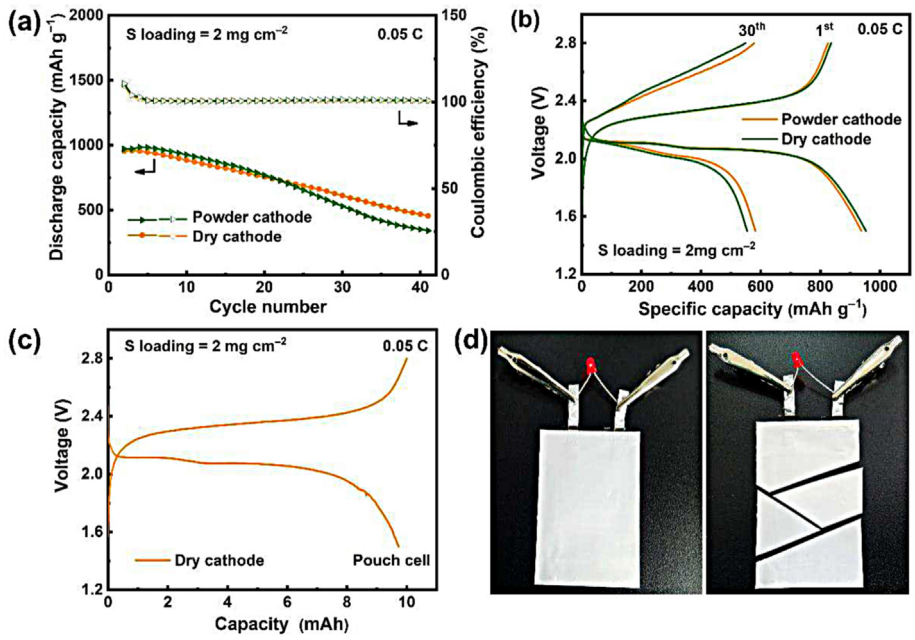

Fig. 5. (a) Cycling performances and (b) corresponding charge–discharge voltage profiles of all-solid-state lithium-sulfur mold cells using powder cathode and sheet-type dry cathode at 0.05 C and 60 °C. (c) The charge–discharge voltage profiles of all-solid-state lithium-sulfur pouch cells with sheet-type dry cathodes at 0.05 C and 60 °C. The sulfur loading is 2 mg cm^{-2}. (d) Illustration of all-solid-state lithium-sulfur pouch cells tested under harsh conditions.

facilitated charge transport and elevated transformation of discharging products Li_2S to elemental sulfur (Fig. 4b).

The mold cells with sheet-type cathodes also exhibit long-term cycle stability (Fig. 4c). Sheet-type dry cathodes deliver higher 34% order of capacity retention than that of powder electrodes and the discharge capacity (558.9 mAh g^{-1}) also exceeds that (460.3 mAh g^{-1}) of powder cathodes after 50 cycles at 0.1 C. The corresponding galvanostatic charge–discharge voltage profiles also clearly show the apparent differences in charge and discharge voltage plateaus (Fig. 4d). In comparison to sharply intensified voltage polarization for powder cathodes, sheet-type sulfur cathodes exhibit relatively flat plateaus with the increase of cycling, which can be ascribed to the advantages of fibrous binder in mitigating volume changes resulting from the repeated sulfur conversion.

In consideration of the demand for high energy density, thickened composite sulfur cathodes (93 μm) with a high sulfur loading of 2 mg cm^{-2} were prepared by dry electrode technology. As shown in Fig. 5(a and b), with increasing cathode loading, thick-

ened sheet-type cathodes deliver comparable initial discharge capacities of 955.5 mAh g^{-1}. Moreover, thickened sheet-type cathodes also show higher capacity retention after 40 cycles at the rate of 0.05 C, which is attributed to the PTFE fibers in mitigating the volume change. However, when increasing electrode thickness and sulfur loading to 2 mg cm^{-2}, powder cathodes show an apparent capacity drop from 971.7 to 341.8 mAh g^{-1}, considerably attributing to huge volume change during cycling. High cycling stability implies unprecedented advantages of dry electrode technology in preparing thickened sulfur electrodes.

In order to further demonstrate the practical application of sheet-type sulfur cathodes by dry electrode technology, all-solid-state lithium-sulfur monolayer pouch cells were fabricated. As can be seen in Figs. S8 and S9, the open-circuit voltage of the pouch cell is 2.31 V and the initial impedance is only 30 Ω. In addition, it delivers a discharge capacity of 9.2 mAh (Fig. 5c). Even under a harsh test situation, being cut into many pieces, the all-solid-state lithium-sulfur pouch cell still operates well, and a red LED continues to be lighted up (Fig. 5d). It further confirms the high safety of ASSLSBs.

Overall, dry electrode technology exhibits many advantages in the preparation of high-energy solid-state sulfur electrodes, however, there remain challenges. On one hand, the immature multi-component solid mixing process and binder fibrillization process need to be improved. It is difficult to obtain a homogenous mixture among solid active materials and solid ionic/electronic conductivities due to their different densities, especially for scale-up mixing. In addition, fibrillization processes also require powerful shearing equipment. On the other hand, a new and stable binder should be further explored due to the incompatibility and instability of PTFE against Li metal anode, which limits the application of PTFE in the preparation of solid-state electrolyte membranes by a dry process. Therefore, more efforts should be devoted to dry electrode technology in the future.

4. Conclusions

In this work, we demonstrated dry electrode technology in the scalable fabrication of thickened sheet-type sulfur cathodes for ASSLSBs. The sheet-type sulfur cathodes possess excellent film-forming and mechanical properties even with a low binder content of 1 wt%. In addition, due to the unique fibrous distribution of binder in dry electrodes, the composite sulfur cathodes exhibit excellent ionic/electronic conductivities and enhanced reaction kinetics. Besides, this fibrous connection between cathode materials also accommodates the stress during sulfur conversion. As a result, ASSLSBs with thickened sulfur cathodes (93 μm) even with high sulfur loading of up to 2 mg cm^{-2} show outstanding rate performance and cycle stability. Moreover, practical all-solid-state lithium-sulfur pouch cells with a high capacity of 9.2 mAh were also demonstrated and exhibited high safety features. Therefore, this work paves a way for scalable fabrication of thickened sulfur cathode and will promote the practical applications of ASSLSBs.

Declaration of competing interest

The authors declare that they have no known competing financial interests or personal relationships that could have appeared to influence the work reported in this paper.

Acknowledgments

This work was supported by the National Key Research and Development Program of China (2021YFB2500300), the National Natural Science Foundation of China (22075029, 22108151, 22109084) and the China Postdoctoral Science Foundation (2021TQ0164).

Appendix A. Supplementary data

Supplementary data to this article can be found online at https://doi.org/10.1016/j.jechem.2022.04.048.

References

[1] L.-Z. Fan, H. He, C.-W. Nan, Nat. Rev. Mater. 6 (2021) 1003–1019.
[2] Y. Qin, X. Chen, A. Tomaszewska, H. Chen, Y. Wei, H. Zhu, Y. Li, Z. Cui, J. Huang, J. Du, X. Han, L. Lu, B. Wu, K. Sun, Q. Zhang, M. Ouyang, Cell Rep. Phys. Sci. 3 (2022) 100708.
[3] X.B. Cheng, H. Liu, H. Yuan, H.J. Peng, C. Tang, J.Q. Huang, Q. Zhang, SusMat. 1 (2021) 38–50.
[4] H. Ye, D. Lei, L. Shen, B. Ni, B. Li, F. Kang, Y.-B. He, Chin. Chem. Lett. 31 (2020) 570–574.
[5] J. Liu, R. Xu, C. Yan, H. Yuan, J.-F. Ding, Y. Xiao, T.-Q. Yuan, J.-Q. Huang, Energy Storage Mater. 30 (2020) 27–33.
[6] Y. Xiao, R. Xu, L. Xu, J.-F. Ding, J.-Q. Huang, Energy Mater. 1 (2021) 100013.
[7] X. Shen, X.-Q. Zhang, F. Ding, J.-Q. Huang, R. Xu, X. Chen, C. Yan, F.-Y. Su, C.-M. Chen, X. Liu, Q. Zhang, Energy Mater. Adv. 2021 (2021) 1205324.
[8] D.-W. Park, N.A. Cañas, N. Wagner, K.A. Friedrich, J. Power Sources 306 (2016) 758–763.
[9] C. Wang, R. Yu, H. Duan, Q. Lu, Q. Li, K.R. Adair, D. Bao, Y. Liu, R. Yang, J. Wang, S. Zhao, H. Huang, X. Sun, ACS Energy Lett. 7 (2022) 410–416.
[10] B. Ludwig, Z. Zheng, W. Shou, Y. Wang, H. Pan, Sci. Rep. 6 (2016) 23150.
[11] Y. Kuang, C. Chen, D. Kirsch, L. Hu, Adv. Energy Mater. 9 (2019) 1901457.
[12] J. Ding, R. Xu, C. Yan, Y. Xiao, Y. Liang, H. Yuan, J. Huang, Chin. Chem. Lett. 31 (2020) 2339–2342.
[13] T. Jiang, P. He, G. Wang, Y. Shen, C.W. Nan, L.Z. Fan, Adv. Energy Mater. 10 (2020) 1903376.
[14] M.X. Wang, Y.L. Wu, M. Qiu, X. Li, C.P. Li, R.L. Li, J.B. He, G.G. Lin, Q.R. Qian, Z.H. Wen, X.Y. Li, Z.Q. Wang, Q. Chen, Q.H. Chen, J.H. Lee, Y.W. Mai, Y.M. Chen, J. Energy Chem. 61 (2021) 253–268.
[15] S. Thieme, J. Bruckner, I. Bauer, M. Oschatz, L. Borchardt, H. Althues, S. Kaskel, J. Mater. Chem. A 1 (2013) 9225–9234.
[16] J. Liu, H. Yuan, H. Liu, C.Z. Zhao, Y. Lu, X.B. Cheng, J.Q. Huang, Q. Zhang, Adv. Energy Mater. 12 (2022) 2100748.
[17] J.K. Hu, P.G. He, B.C. Zhang, B.Y. Wang, L.Z. Fan, Energy Storage Mater. 26 (2020) 283–289.
[18] Y. Lu, C.Z. Zhao, H. Yuan, X.B. Cheng, J.Q. Huang, Q. Zhang, Adv. Funct. Mater. 31 (2021) 2009925.
[19] Y. Lu, C.-Z. Zhao, R. Zhang, H. Yuan, L.-P. Hou, Z.-H. Fu, X. Chen, J.-Q. Huang, Q. Zhang, Sci. Adv. 7 (2021) eabi5520.
[20] S. Wang, Q. Sun, W. Peng, Y. Ma, Y. Zhou, D. Song, H. Zhang, X. Shi, C. Li, L. Zhang, J. Energy Chem. 58 (2021) 85–93.
[21] H. Liu, X. Cheng, C. Yan, Z. Li, C. Zhao, R. Xiang, H. Yuan, J. Huang, E. Kuzmina, E. Karaseva, V. Kolosnitsyn, Q. Zhang, iEnergy 1 (2022) 72-81.
[22] J.-H. Jiang, A.-B. Wang, W.-K. Wang, Z.-Q. Jin, L.-Z. Fan, J. Energy Chem. 46 (2020) 114–122.
[23] S. Sun, C.-Z. Zhao, H. Yuan, Y. Lu, J.-K. Hu, J.-Q. Huang, Q. Zhang, Mater. Futures 1 (2022) 012101.
[24] Z.-H. Fu, X. Chen, C.-Z. Zhao, H. Yuan, R. Zhang, X. Shen, X.-X. Ma, Y. Lu, Q.-B. Liu, L.-Z. Fan, Q. Zhang, Energy Fuels 35 (2021) 10210–10218.
[25] X. Chen, H. Ji, Z. Rao, L. Yuan, Y. Shen, H. Xu, Z. Li, Y. Huang, Adv. Energy Mater. 12 (2021) 2102774.
[26] X. Gao, X. Zheng, Y. Tsao, P. Zhang, X. Xiao, Y. Ye, J. Li, Y. Yang, R. Xu, Z. Bao, Y. Cui, J. Am. Chem. Soc. 143 (2021) 18188–18195.
[27] H. Liu, T. Li, X. Xu, P. Shi, X. Zhang, R. Xu, X. Cheng, J. Huang, Chin. J. Chem. Eng. 37 (2021) 152–158.
[28] F.N. Jiang, S.J. Yang, H. Liu, X.B. Cheng, L. Liu, R. Xiang, Q. Zhang, S. Kaskel, J.Q. Huang, SusMat. 1 (2021) 506–536.
[29] J. Xu, L. Liu, N. Yao, F. Wu, H. Li, L. Chen, Mater. Today Nano 8 (2019) 100048.
[30] K. Lee, S. Kim, J. Park, S.H. Park, A. Coskun, D.S. Jung, W. Cho, J.W. Choi, J. Electrochem. Soc. 164 (2017) A2075–A2081.
[31] D.H. Kim, Y.-H. Lee, Y.B. Song, H. Kwak, S.-Y. Lee, Y.S. Jung, ACS Energy Lett. 5 (2020) 718–727.
[32] Z.-H. Fu, X. Chen, N. Yao, X. Shen, X.-X. Ma, S. Feng, S. Wang, R. Zhang, L. Zhang, Q. Zhang, J. Energy Chem. 70 (2022) 59–66.
[33] Q. Yu, K. Jiang, C. Yu, X. Chen, C. Zhang, Y. Yao, B. Jiang, H. Long, Chin. Chem. Lett. 32 (2021) 2659–2678.
[34] Y. Li, D.C. Zhang, X.J. Xu, Z.S. Wang, Z.B. Liu, J.D. Shen, J. Liu, M. Zhu, J. Energy Chem. 60 (2021) 32–60.
[35] S.-B. Hong, Y.-J. Lee, U.-H. Kim, C. Bak, Y.M. Lee, W. Cho, H.J. Hah, Y.-K. Sun, D.-W. Kim, ACS Energy Lett. 7 (2022) 1092–1100.
[36] Y. Lu, C.-Z. Zhao, H. Yuan, J.-K. Hu, J.-Q. Huang, Q. Zhang, Matter 5 (2022) 876–898.
[37] J. Lee, T. Lee, K. Char, K.J. Kim, J.W. Choi, Acc. Chem. Res. 54 (2021) 3390–3402.
[38] Z. Zhang, L. Wu, D. Zhou, W. Weng, X. Yao, Nano Lett. 21 (2021) 5233–5239.

[39] F. Hippauf, B. Schumm, S. Doerfler, H. Althues, S. Fujiki, T. Shiratsuchi, T. Tsujimura, Y. Aihara, S. Kaskel, Energy Storage Mater. 21 (2019) 390–398.
[40] Y.-G. Lee, S. Fujiki, C. Jung, N. Suzuki, N. Yashiro, R. Omoda, D.-S. Ko, T. Shiratsuchi, T. Sugimoto, S. Ryu, J.H. Ku, T. Watanabe, Y. Park, Y. Aihara, D. Im, I. T. Han, Nat. Energy 5 (2020) 299–308.
[41] S. Ohno, R. Koerver, G. Dewald, C. Rosenbach, P. Titscher, D. Steckermeier, A. Kwade, J. Janek, W.G. Zeier, Chem. Mater. 31 (2019) 2930–2940.
[42] Y.-X. Song, J. Wan, H.-J. Guo, Y. Shi, X.-C. Hu, B. Liu, H.-J. Yan, R. Wen, L.-J. Wan, Energy Storage Mater. 41 (2021) 642–649.
[43] H. Liu, X. Cheng, Y. Chong, H. Yuan, J.-Q. Huang, Q. Zhang, Particuology 57 (2021) 56–71.
[44] D. Cao, Q. Li, X. Sun, Y. Wang, X. Zhao, E. Cakmak, W. Liang, A. Anderson, S. Ozcan, H. Zhu, Adv. Mater. 33 (2021) e2105505.
[45] L.-P. Hou, H. Yuan, C.-Z. Zhao, L. Xu, G.-L. Zhu, H.-X. Nan, X.-B. Cheng, Q.-B. Liu, C.-X. He, J.-Q. Huang, Q. Zhang, Energy Storage Mater. 25 (2020) 436–442.
[46] Q. Zhang, N. Huang, Z. Huang, L.T. Cai, J.H. Wu, X.Y. Yao, J. Energy Chem. 40 (2020) 151–155.
[47] L. Xu, Y. Lu, C.Z. Zhao, H. Yuan, G.L. Zhu, L.P. Hou, Q. Zhang, J.Q. Huang, Adv. Energy Mater. 11 (2021) 2002360.
[48] B. Zhao, L. Ma, K. Wu, M. Cao, M. Xu, X. Zhang, W. Liu, J. Chen, Chin. Chem. Lett. 32 (2021) 125–131.
[49] X. Yao, N. Huang, F. Han, Q. Zhang, H. Wan, J.P. Mwizerwa, C. Wang, X. Xu, Adv. Energy Mater. 7 (2017) 1602923.